Spatial Resolution of Current Distribution inside a Radio Frequency Resonator

Adrian Beckert
11-917-788

November 13, 2014

Abstract

A laser scanning microscope was used to image a superconducting Nb resonator in the optical range. Additionally the influence of the laser on the transmission line signal was used to spatially resolve the current mode structure in the resonator and the current distribution across the conductor. This prevents future projects of lengthy and higher order simulations of complex resonator systems.

Contents

1 Introduction

For building a quantum computer consisting of microwave resonators and qubits it's of crucial interest to know the mode structure of the current distribution inside the resonators since qubits are generally field sensitive [1]. According to the desired coupling mechanism and strength the qubit has to be placed on different locations on the chip depending on the mode structure. For simple geometries theory provides analytical solutions whereas for more complex systems such as coupled or spiral-shaped resonators the problem isn't analytically solvable anymore. Hence numerical simulations have to be employed. However, given the fact that the more resonator are coupled the more computing resources such as running time or hardware capacity are required. Furthermore taking into account environmental influences such as different sample holders or the proper grounding of the sample itself would increase simulation costs. Therefore it's very convenient if the current distribution can directly be measured by a laser scanning microscope (LSM). The LSM was chosen because as described in [2] in more detail, the various advantages of a LSM consist in the broad application range of a LSM beside optical imaging and the electrical neutrality of the particles (photons) involved into the imaging process.
The main question to be answered is how to spatially resolve the current distribution inside a resonator with a LSM. The present thesis gives a brief theory introduction to the LSM methods and focuses on how to map a sample with a LSM and how to extract desired informations such as the reflection image or the current distribution

1.1 Theory

As the name Laser Scanning Microscope implies, the imaging process is done with a laser. The measuring process, more precisely the photon impact on the surface of the sample, will influence the imaged system. Since in the present thesis a superconducting sample was used, the impact of the photons on the surface causes Cooper pairs to break up which has two effects which will be considered separately.

1.1.1 Change of kinetic inductance

The Hamiltonian $\mathcal{H}$ of a resonator in $\mathbb{R}^3$ is given by

$$\mathcal{H} = \int\limits_{\mathbb{R}^3} \left[\frac{C(x)V(x)^2}{2} + \frac{L(x)I(x)^2}{2} \right] d^3\mathrm{x} \tag{1}$$

where $C(x)$ denotes the capacitance, $V(x)$ the voltage, $L(x)$ the inductance and $I(x)$ the current. If the resonator is assumed to be one dimensional and parametrised by x, the Hamiltonian $\mathcal{H}$ of this resonator simplifies to

$$\mathcal{H} = \int\limits_{0}^{l} \left[\frac{C(x)V(x)^2}{2} + \frac{L(x)I(x)^2}{2} \right] d\mathrm{x} \tag{2}$$

where l denotes the length of the one-dimensional resonator. This assumption is a good approximation since in the case of this thesis width ($\approx 10\mu$m) and height (≈ 150nm) of the resonator are much smaller than the length (≈ 10mm) of the resonator.
Since the laser spot diameter d_L is much smaller than the characteristic length of the system, the resonance wave length λ ($d_\mathrm{L} \ll \lambda$), the laser induced change of the kinetic inductance can be assumed to be $\Delta L\delta(x - x_L)$ with x_L the laser spot position and ΔL the proportionality constant. The inductance is thus given by

$$L(x) = L_0(x) + \Delta L\delta(x - x_L)$$

where $L_0(x)$ indicates the ordinary inductance of the resonator without the laser influence. It is assumed that the laser induced change of the inductance is the same everywhere. Inserting this into eq. 2 we obtain

$$\int \frac{C(x)V(x)^2}{2} d\mathrm{x} + \int \frac{L_0(x)I(x)^2}{2} d\mathrm{x} + \int \frac{I(x)^2\Delta L\delta(x - x_L)}{2} d\mathrm{x}$$

for the Hamiltonian. The first two terms resemble the unperturbed harmonic oscillator which yields

$$E = \hbar\omega \left(\langle n \rangle + \frac{1}{2} \right) \tag{3}$$

for the energy and the last term can be calculated to

$$E = \frac{\Delta L I(x_L)^2}{2} \tag{4}$$

for the change of energy induced by the laser. The total energy of the resonator is thus given by

$$E = \hbar\omega \left(\langle n \rangle + \frac{1}{2} \right) + \frac{\Delta L I(x_L)^2}{2}. \tag{5}$$

and the change of energy $\Delta E = \hbar\Delta\omega$ is therefore proportional to

$$\Delta E \propto I(x)^2 \tag{6}$$

which in case of

$$I(x) = I_0 \cos(x) \tag{7}$$

yields

$$\Delta E \propto I_0^2 \cos^2(x).$$

1.1.2 Change of Resistance

The energy dissipation of a resonator depends on internal factors such as the conductance or external factors such as geometry. Since the geometry is given, the following consideration focuses on the internal factors which are changed by the laser influence.
Similar to section 1.1.1 the laser spot is assumed to be much smaller than the resonance wavelength and again the resonator is assumed to be one-dimensional and parametrised by x. Then the position dependent resonator resistance $R(x)$ can be written as

$$R(x) = R_0(x) + \delta(x - x_L)\Delta R \tag{8}$$

with x_L the laser position and R_0 the resistance of the non-influenced resonator. Since the energy dissipation of the resonator is given by

$$\Delta P = \int I^2(x) R(x) d\mathrm{x} \tag{9}$$

the dissipation changes to

$$\Delta P = \Delta P_0 + I^2(x_L)\Delta R \tag{10}$$

using eq. 8. After [3] p.274 the quality factor Q is defined as:

$$Q = \omega \frac{\text{average energy stored}}{\text{energy loss/second}} \tag{11}$$

or in terms of power

$$Q = \frac{E\omega}{\Delta P} \tag{12}$$

is given for the quality factor Q. Therewith it follows that

$$Q \propto \cos^2(x) \tag{13}$$

in case of periodic current as given in eq. 7.

2 Sample and measurement setup

2.1 Sample

The sample consists of a $2x7$mm superconducting Niobium chip with 6 resonators of different resonance frequencies. In fig. 1 a scheme of the chip design can be found. The resonators are capacitively coupled with different

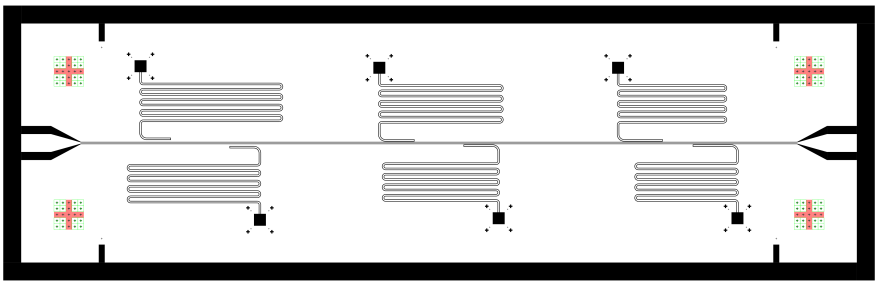

Figure 1: Scheme of the sample

coupling constants to the transmission line. Th Nb thickness is 150nm and the structures were made by photo-lithography. In fig. 2 the measured transmission spectrum of the chip is shown. The six resonances were observed at frequencies:

$$6.36, 6.50, 7.22, 7.64, 8.07, 8.49 \text{ GHz} \tag{14}$$

Fig. 2 shows the transmission line of the sample chip. The resonance frequencies indicated in 14 can be observed as well.

2.2 Measurement setup

Sample location The sample was mounted on a copper sample holder in a pulse tube fridge with a base temperature of 4.2K. The temperature was stabilized at 4.5K with a proportional-integral-derivative (PID) controller. Fig. 3 shows the position of the sample on the sample-holder relative to the scanning area of the LSM.

2.2.1 Laser scanning microscope

Lens positioning system The lenses were positioned with a piezo based 3D positioning system from attocube® with 5mm×5mm×5mm total moving range.

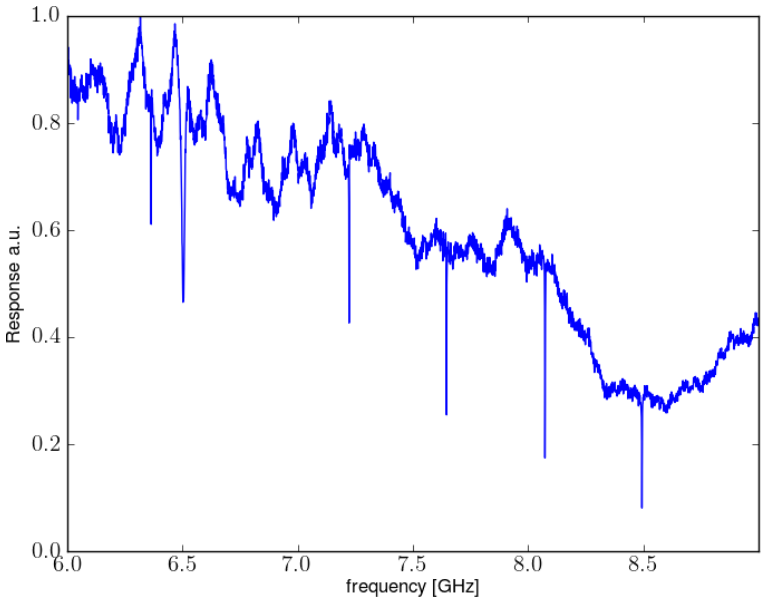

Figure 2: Resonance frequencies of the sample chip

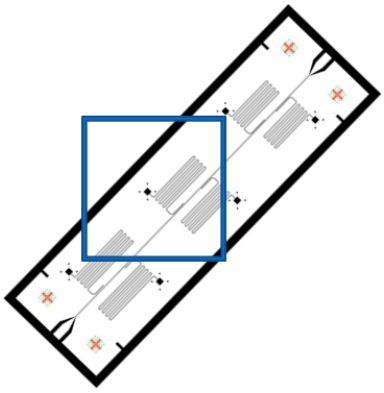

Figure 3: Sample position on the base plate with LSM scanning area

Laser beam In fig. 4 a scheme of the following description is shown. The laser beam in the blue range ($460 - 480$nm), produced by a diode laser was collimated and led with mirrors to an acusto optical modulator (AOM). Afterwards the beam was led via a fiber coupler (f.c.) from the first laser shield box to the second laser shield box. The beam was subsequently led on a $92 : 8$ beam splitter i.e. 92% of the intensity passed and 8% was reflected

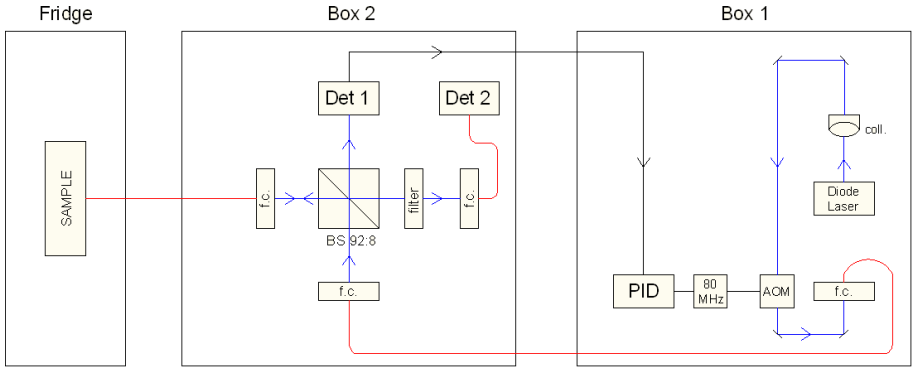

Figure 4: Scheme of the laser beam setup

at 90^o degree.
The passing beam part (92% of the initial beam) fell on a detector (Det 1) whose signal was fed to the PID controller. This PID controller was connected to a 80MHz signal generator producing the signal for the AOM. Thus this loop was for stabilizing the laser power.
The reflected part at the beam splitter (8% of the initial beam) was led via a fiber coupler into the fridge where the beam hit the surface of the chip after passing a system of focal lenses. The light reflected from the sample was led on the same way out of the fridge again on the beam splitter. The passing part was filtered and then led via a fiber coupler to a detector (Det 2). The filter reduced the intensity of the beam in order to avoid detector saturation. The voltage given from detector 2 was read out by the computer.

2.2.2 Electrical circuit

In fig. 5 a scheme of the RF-circuit can be found. A simplified version of the optical circuit is also shown.
The signal of the radiofrequency signal generator 1 (SG1) was attenuated by 60dB and then led on the chip via coaxial cables. The signal transmitted through the chip was amplified using a low-temperature HEMT amplifier at 4K and afterwards led onto a second amplifier at room temperature before passing a band pass filter with a range of $6 - 11$GHz. Subsequently, the signal was mixed with the signal of SG2. The cosine part was led after being low pass filtered with 450MHz to a field programmable gate array (FPGA) and then read out by the computer. The sine part was led to a 1.9MHz low pass filter and then led to the ASC500, the LSM stepper control system with a built-in lock-in amplifier function.

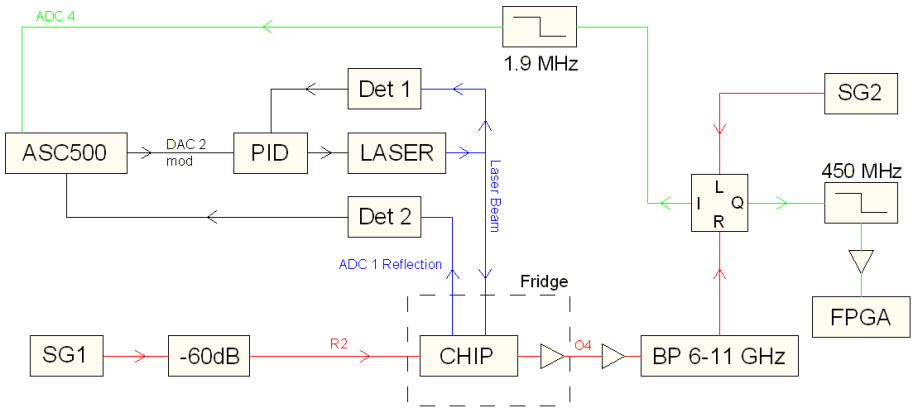

Figure 5: Scheme of the RF-circuit including simplified fig. 4

3 Reflection Measurement

3.1 Measuring process

First the LSM was set at the starting point of the scanning area and afterwards tuned in z-direction (perpendicular to the sample plane) to find the focal point. Since the chip plane was not mounted perfectly perpendicular to the laser beam, the focal point depended on the (x, y)-position. Therefore it was necessary to adjust the the point of the LSM such that it was in the focal point with some minor deviance throughout the whole scanning area. This was achieved by setting the LSM in the approximate center of the scanning area into the exact focal point. The focal point was found by scanning at specific (x, y)-coordinates and varying the z-coordinate of the LSM point. The z-coordinate with maximum reflection signal corresponds to the focal point.
In order to prevent detector voltage saturation, depending on the location of the scanning area on the chip, different laser powers and/or filters (described in subsection 2.2.1) had to be applied. In regions with higher reflectivity and better signal less laser power and stronger filters and vice versa.
After laser power and focal point were properly tuned, step size and frequency of the x and y steppers had to be set. The frequency corresponds to the velocity of the steppers.
The built-in scanning function of the positioning system control software applies a specific procedure during a scanning process (scan a specific area on the chip). For the following demonstration of the procedure it is assumed, that a rectangular area between the points $(0, 0)$ and (x, y) has to

be scanned. First, the x-stepper moves along the x-coordinate to $(x, 0)$. After having reached $(x, 0)$ the x-stepper moves exactly the same way back to $(0, 0)$. Then the y-stepper moves to $(0, \Delta y)$ where Δy denotes the y step size. Now the algorithm is performed this way until the LSM point reaches (x, y). Having reached (x, y) the y-stepper moves first to $(0, y)$ and then to $(0, 0)$ again.
The positioning system control software provides two different scanning modes. One for small scanning areas up to $(50\mu\text{m} \times 50\mu\text{m})$ where the LSM point is moved without the piezo stepping technique and one for large i.e. one side of the scanning area is $> 50\mu$m where the piezo stepping technique is applied. For both modes, the same scanning algorithm is applied with one exception. While the x-positioner moves e.g. from $(x, 0)$ back to $(0, 0)$ a second measurement of the same line is performed. At the end there are two scans of the same area available, one scanned in right direction and one scanned in left direction.

3.2 Results

Figure 6 shows the reflection image of the upper central resonator of the chip (see fig. 3 for details). The horizontal and vertical axes correspond to the stepper position readings. The z-axis, represented in grayscale refers to the detector voltage which is proportional to the reflected light intensity.
The resonator is not as precisely mapped as indicated in fig. 1. The straight parts of the resonator show well, that the image is blurred and wiggled. Additionally discontinuous changes in intensity in x-direction appear.

3.3 Analysis and Discussion

Figure 6 shows that the superconducting parts of the chip have higher reflectivity than the non-reflecting substrate. Similarly, the copper base plate of the sample holder has very low reflectivity compared to the superconducting parts of the chip.
That straight parts of the resonator appear wiggled and blurred is due to two reasons. In order to reduce the scanning time the resolution was chosen to be $2.5\frac{\mu\text{m}}{px}$. The steppers obey not exactly to the moving commands of the control system. Sometimes they get stuck and move just 1-3 scanning lines later to the actual position. Although this effect was numerically corrected it contributes to the wiggled impression of figure 6.
The discontinuous change in intensity in x-direction is due to temperature changes and other unknown environmental influences. Since the focal point

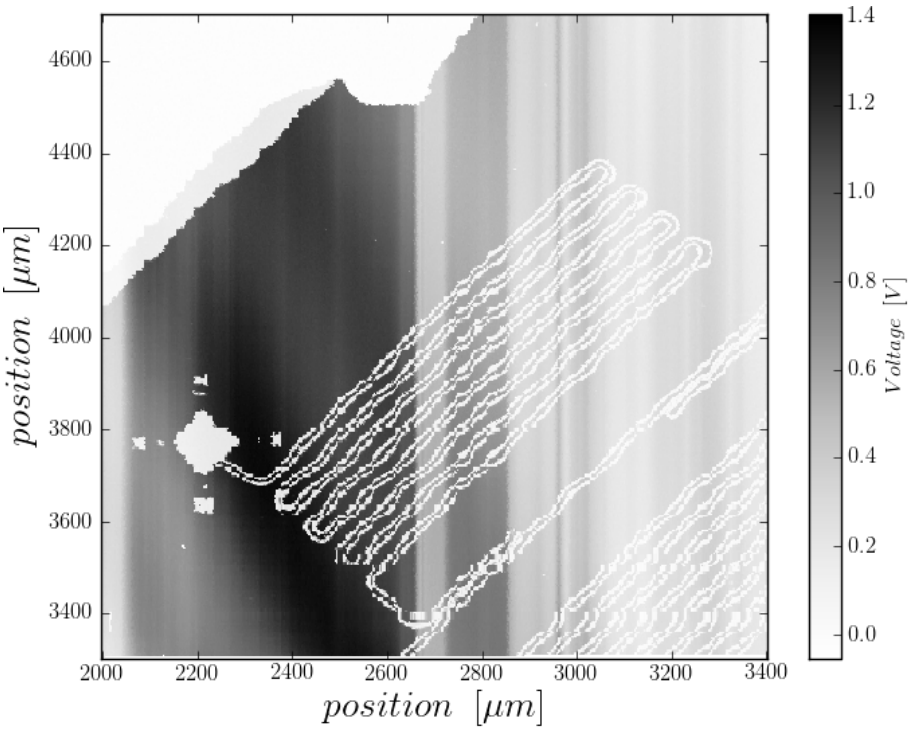

Figure 6: Reflection image of one central resonator of the sample chip

had to be adjusted in the μm-range, already slight changes influence the measured reflection intensity.

4 Mode structure of the resonator

4.1 Measuring process

Intorduction As described in sec 1.1.1 and 1.1.2 the laser influences the resonator. In fig. 7 the resonance in the scanning area of the LSM is shown for different laser powers. The changes of the transmission amplitude, indicated

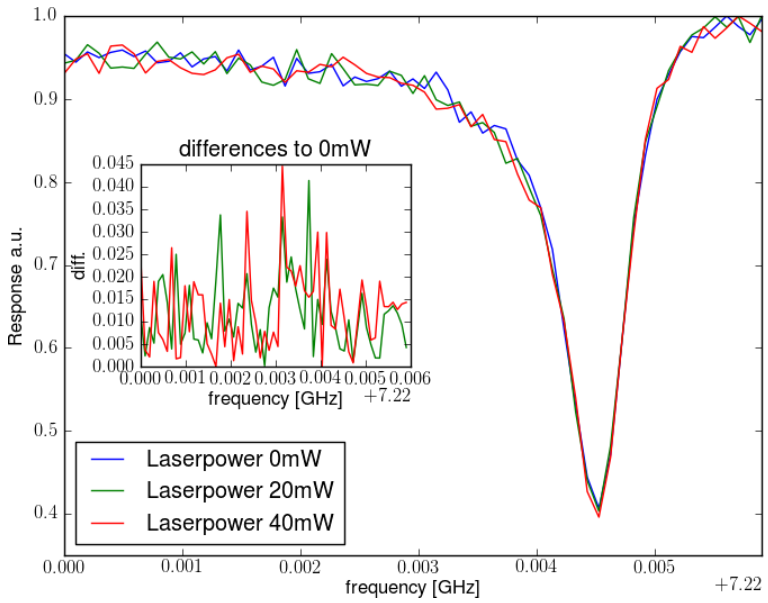

Figure 7: Transmission line as a function of different laser powers. Inset: differences to 0mW laser power

in fig. 7, were very small. In order to detect such small changes it was decided to use a Lock-in-Amplifier.

Laser induced transmission line change measurement Figure 17 in the appendix shows, that the 7.22GHz transmission line changes during a measurement. This originates from a temperature increase during the measuring process. As fig. 17 shows as well, after some time, the resonance stays constantly at one frequency. This behaviour was observed while the base temperature of the fridge was at 4.2K. Therefore as described in section 2.2, a PID controlled temperature stabilisation was realised at 4.5K, so that there was no temperature increase anymore due to the stepper movement during the measurement process.

Before the resonator was scanned, the exact position of the resonance was measured with CleanSweep. Afterwards the frequency of signal generator 1 and 2 was set approximately to the frequency of the steepest point in the resonance dip. For fig. 7 7.242GHz would have been the frequency. The frequency was chosen this way in order to measure at the most sensitive point for shifts and/or broadening of the resonance dip in frequency.
The laser power was modulated with 2.534kHz at a power of 200mV and an amplitude of 180mV. The built-in lock-in amplitude function of the ASC500 allowed to measure the change in the transmission line signal. The integration time of the lock-in was set to 6.314ms.

4.2 Results

Figure 8 shows the result of the measurement process described in section 4.1. The axes of the plot correspond again to the axes of the laser scanning

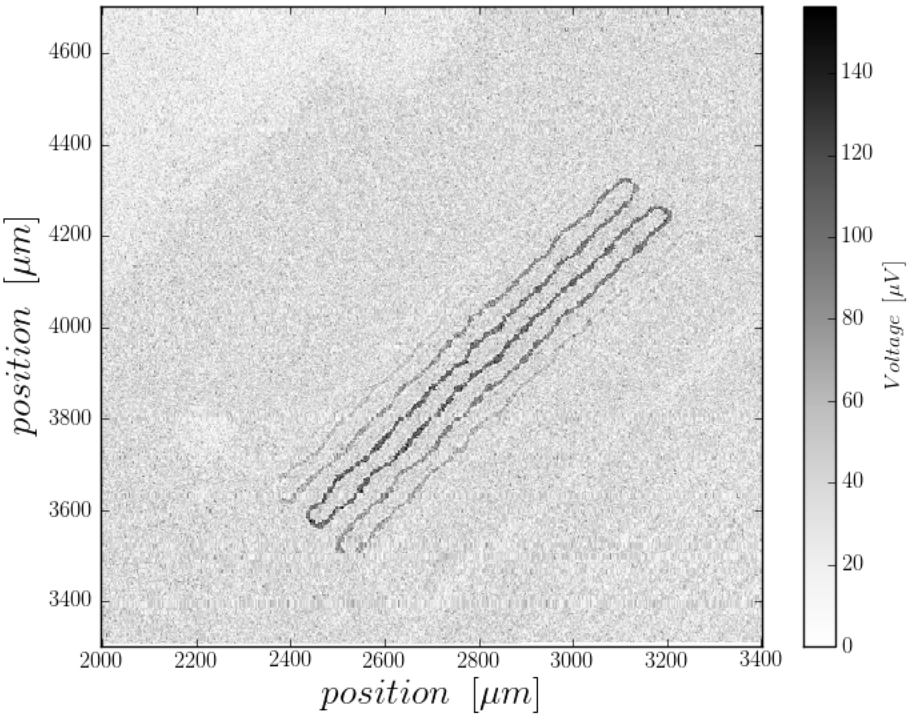

Figure 8: Current distribution of the resonator

microscope and the z-axis is the detected signal from the lock-in amplifier.

The scanning range is 1.4×1.4mm with 561×561 pixel resolution. The image appears again wiggled, similar to the optical image shown in fig. 6.
In addition to the resonator the other structures of the chip as well as the edge can be seen (compare with fig. 6).

4.3 Analysis and discussion

Since the resolution and the stepper disobedience to the control system stay the same, this explains the blur of the image.
The mapped resonator is in a good approximation a simple 1D resonator and therefore the mode structure of the current distribution is just $\propto \cos^2$ along the resonator length. Indeed, fig. 9 shows along the resonator length from the beginning of the first line to the end of the last line the detected signal and a least squares fit. Although the values spread a lot, fig. 9 shows,

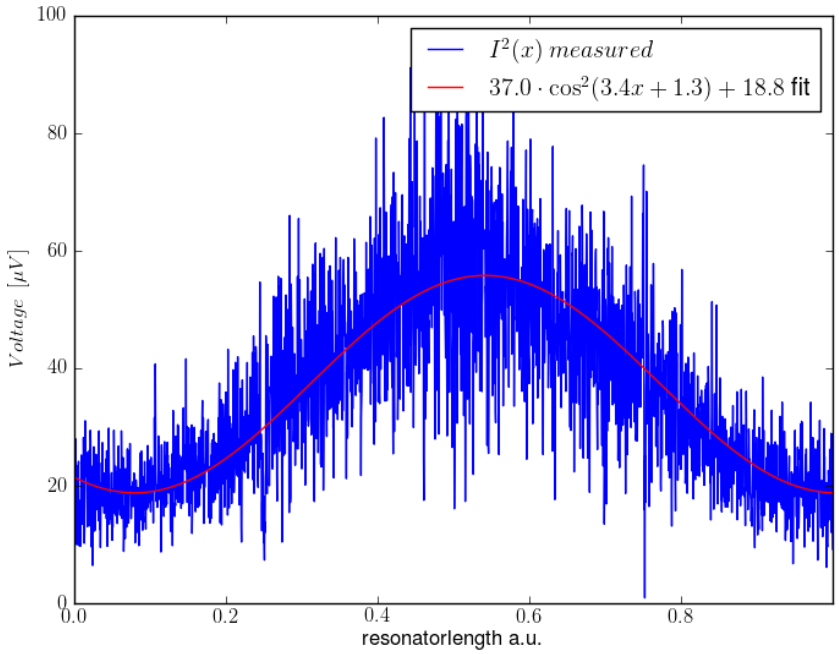

Figure 9: Current distribution along the resonator with least squares fit

that the measured change in the signal is proportional to $\cos^2$ and therefore likely the current distribution along the resonator length.
It is important to understand why the other structures of the chip can be seen although the signal should be $\propto I^2$ and off the resonator $I = 0$ yields. The direction of the resonance change is not known, so it is impossible to know

what exactly happened beside the resonator. One possible explanation is, that the laser power was so high, that it heated up more than just a narrow spot and due to heat convection disturbed the measurement. Given the fact that the resolution is nevertheless quite high disturbance due to heat convection seems less probable. If this really was the only reason, the whole image would be blurred and the signal to noise ration close to 1. Another reason could be a cross talk between optical and microwave signals inside the ASC500 device.

5 Current distribution in resonator cross section

5.1 Measuring process

For the detailed scans the same measuring procedure as described in section 4.1 was used except the lock-in integration time was set differently and the scanning area was smaller. The lock-in integration time was set to 101ms

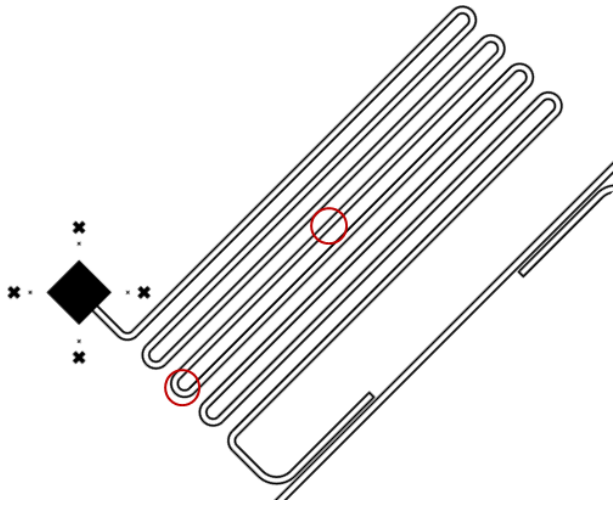

Figure 10: Location of the detailed scans indicated with red circles on a detail of the resonator scheme

and the LSM scanning area was set to $40 \times 40 \mu$m with 200×200 pixels. Since the scanning area was smaller than $50 \mu\text{m} \times 50 \mu$m the step-scanning mode had not to be applied.
Two different locations were selected for the detailed scanning areas. First a straight part in the center of the resonator were the signal was expected to bee higher than at the ends and second a curved part in exactly the center

of the resonator length. In fig. 10 these two locations are indicated with red circles on a detail of the resonator scheme.

5.2 Results

The microwave signal of the straight part is shown in fig. 11 and the curved part in fig. 12.

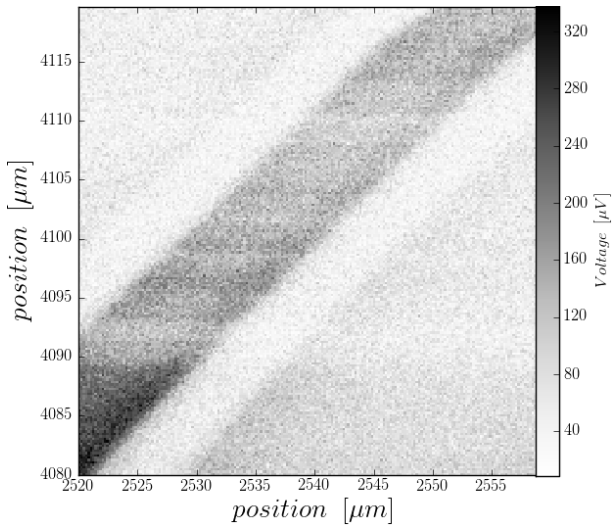

Figure 11: Detail microwave measurement of a center straight part of the resonator

Straight part The (x, y)-axes are again the axes of the LSM and the z-axis displayed in gray-scale corresponds to the measured lock-in signal. The dark part on the diagonal belongs to the resonator line, while the bright parts are the gap between the resonator and the rest of the chip.
Fig. 11 shows in the upper part of the image a slight distortion. From $y \approx 4090\mu$m on, there is a large drop of intensity which is visible in the regime of the resonator but almost hidden for the rest of the chip.

Curved part For the curved part the situation is similar to fig. 11 with respect to the axes and what is observed. In fig. 12 between $x \approx 3800\mu$m and $x \approx 3815\mu$m again a drop of intensity is observed which afresh can be observed in the regime of the resonator but is almost hidden in the noise of the chip parts beside the resonator.

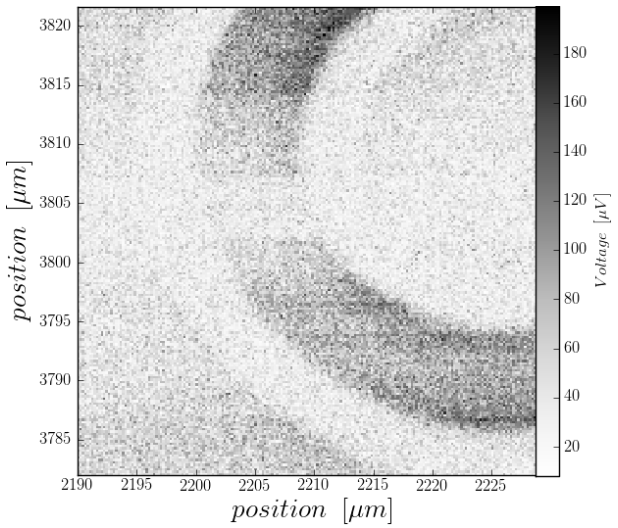

Figure 12: Detail microwave measurement of a center curved part of the resonator

5.3 Analysis and Discussion

Straight part First, the distortion and the intensity drop are considered. The distortion likely results from inaccuracies of the LSM point positioner on the edge range of the scanning field. The drop of intensity originates from changes of the environmental settings. The result of fig. 11 is the result of a long term measurement of several hours. Therefore it is likely that some slight and unknown changes caused the drop of intensity.
In order to analyse fig. 11 regarding the intensity drops the following was done: The detail of $40 \times 40\mu$m is a very small section compared to the extent of the resonator. Therefore it is assumed that the current distribution will not change significantly over the length of the scanned part of the resonator. In order to know the current distribution in across the resonator and to smoothen out the intensity drops and variations, the signal was averaged along the resonator line, shown in fig. 13. Since in the lower right edge of fig. 11 there is only the right side imaged of the resonator line, this region was left out and the averaging started 12μm after the beginning of the image in the direction of the resonator.
Figure 13 shows some interesting features. First, the current distribution in the center of the resonator line is lower than at the edges. Between the edges of the resonator line there is a slight asymmetry in the height of the current

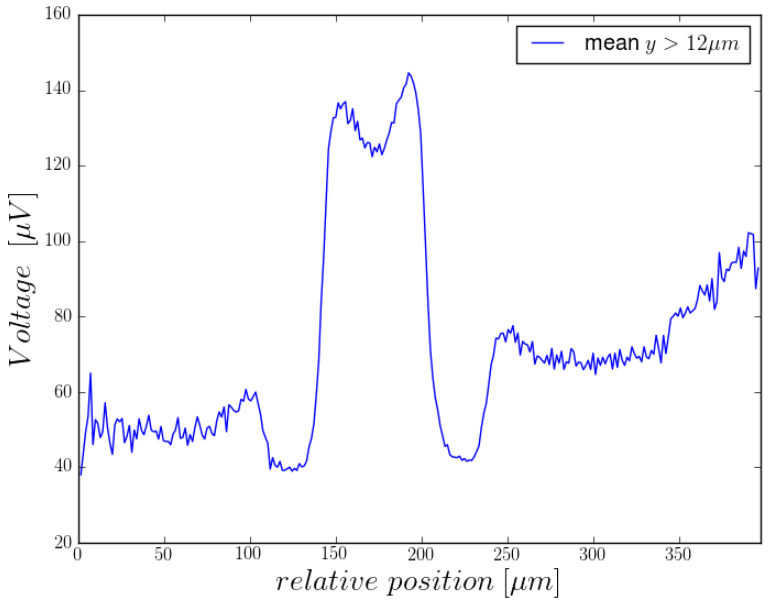

Figure 13: Average along the resonator line

distribution. That the current distribution is lower in the center than on the edges of the conductor may correspond to the skin-effect of a conductor at high frequencies [4]. By contrast, the asymmetry is not predicted by the skin-effect but seems to consist also for the parts off the resonator in fig. 13. Since the noise on the right side of the conductor in fig. 13 is higher than on the left side as well as the current distribution on the right edge of the conductor is higher than on left side there seems to be an (linear?) increasing background. This increasing background may originate from the slight tilting of the sample.
Second, the current distribution off the resonator seems to increase towards the resonator line before the gap. If a 3D plot of the straight part is considered, as shown in fig. 14 the features seen in fig. 13 are confirmed. Even the trend of the current distribution to increase towards the gap between resonator line and the rest of the chip is clearer to see in fig. 14. The origin of the increase of the current distribution towards the resonator line is what is suggested by computer simulations [**?**]. Although in the simulations in [**?**] suggest the current distribution on both sides on the gap to be equally high the increase is suggested to originate from this effect. Thermal conduction and/or crosstalk of microwave and optical components within the ASC500 device may have damped this effect.

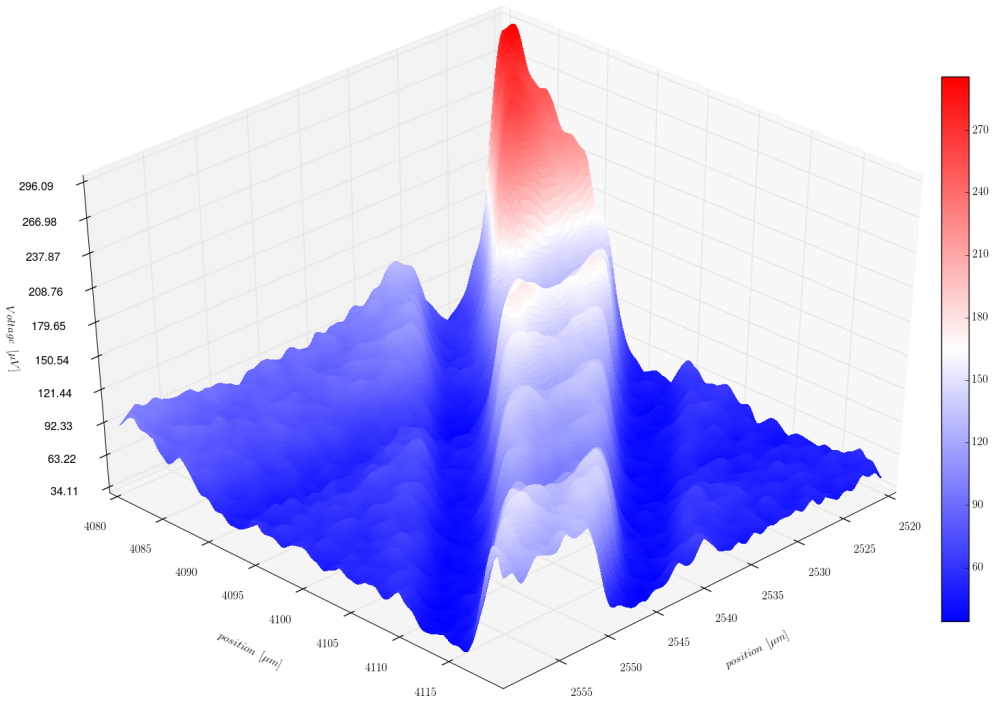

Figure 14: 3D plot of the straight part

Curved part Similar to the straight part in the previous paragraph, the current distribution in the cross section of the resonator line was averaged along the arc. The result of this process can be seen in fig. 15. The red graph in fig. 15 corresponds to the average over a small section in the center of the arc, off the strong intensity change in the upper part of fig. 12.
Similar to the straight part, the current distribution in the center of the resonator is lower than on the edges. The mean along the whole arc shows a more expressed asymmetry between the inner edge and the outer edge. The current distribution on the inner edge of the resonator with the higher curvature seems to be lower than on the outer edge with the lower curvature. The average over the small section drawn in red in fig. 15 shows the same effect but less expressed. Considering fig. 16 shows that this effect is most likely due to the averaging process along the arc. On the left side of figure 16 the inner side of the resonator shows a higher current distribution while on the right side of the figure the outer side reveals a higher current distribution. Therefore this effect has not to be considered as important. Furthermore since there was an averaging along the arc the increasing background seen

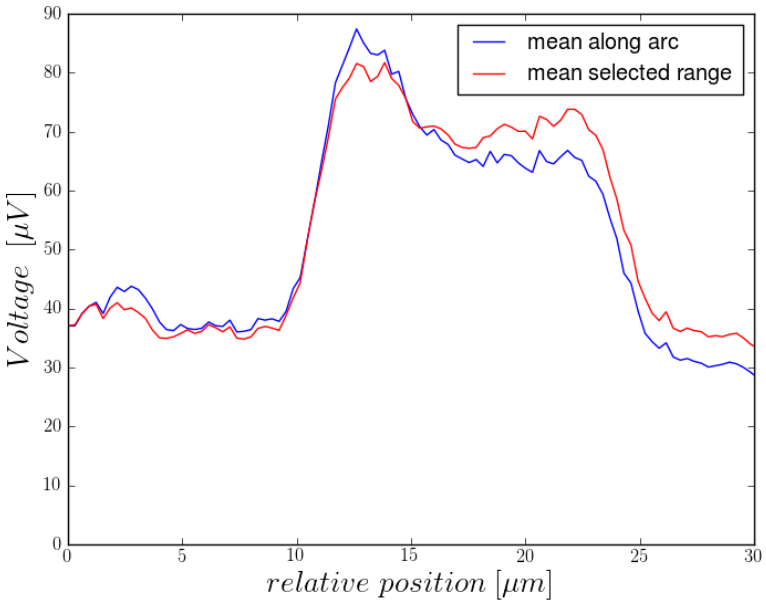

Figure 15: Average along the resonator line

in fig. 13 and mentioned in the paragraph before should not appear. Indeed in fig.15 the noise level of both sides of the resonator are approximately at the same level.
A fact that astonishes is, that the gap between the resonator line and the rest of the chip is fainter than in fig. 13. Having a look at figure 16 lets suppose that this effect is not as expressed as one could think from fig. 15. This effect may come from an improper averaging along the arc i.e. that within the averaging process which included a nonlinear mapping of the arc onto a straight line edge values of the gap were included. Additionally its obvious from figure 16 that in the central regime of the arc large parts of the gap are really not well expressed which caused the average depth of the gap to decrease.
Having another look at the 3D plot of the curved part in fig. 16 reveals some additional information which could not be observed in figs. 12 and 15. The gap between the resonator line and the side parts on the chip can be observed in more detail. Additionally the increase of the current distribution towards the gap can be clearly observed in fig. 16 on the right side and faintly on the left side. Again the current distribution is higher on the edges as in the center of the resonator curve. It is self-evident, that the decrease of intensity, which seems confined just to the resonator line, influences the averaging too

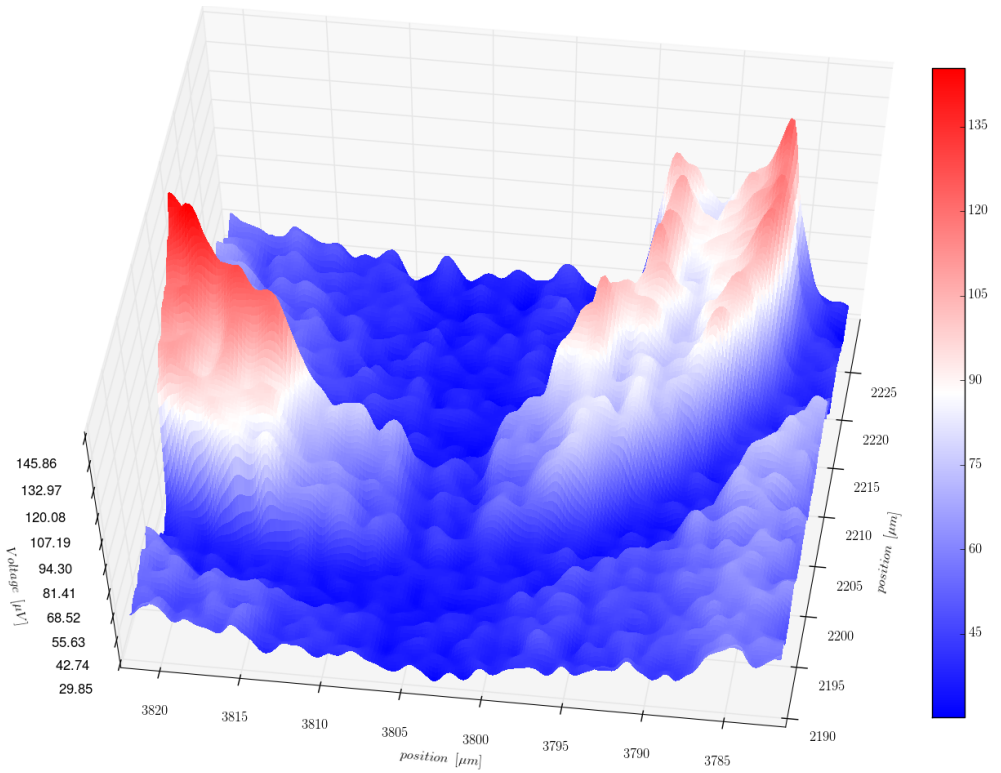

Figure 16: 3D plot of the curved part

much and further improvements of measurement techniques are needed.

6 Conclusion and Outlook

The sample chip could be optically imaged. Concerning the current distribution there is strong evidence that the measured quantity really corresponds to the current distribution. The mode structure of a simple resonator could be mapped as well as the current distribution over a cross section of the resonator line for straight and for curved parts of the resonator. Nevertheless there are several questions which couldn't yet be answered and therefore impede a thorough interpretation of the data. The following questions have to be answered, if the performed experiments want to be understood in a more quantitative way:

- How large is the laser spot on the sample?
- How much energy is deposed on the surface by the laser (as a function of the applied laser voltage)?
- How does the deposed energy influence the quasi-particle density and therefore the resistance and inductance of the superconductor?
- How does the transmission line behave as a function of laser power?
- How can the contrast between "laser on" and "laser off" be increased?

If the previous mentioned questions are answered, more complicated systems such as lumped element structures, spirals or coupled resonators can be mapped and quantitatively analysed.

7 Appendix

References

[1] R. J. Schoelkopf and S. M. Girvin, Nature **451**, 664-669 (2008)

[2] A. P. Zhuravel *et al.*, Low Temperature Physics: **32**, 592 (2006)

[3] D.M. Pozar, Micorwave engineering, (John Wiley & Sons, 2012)

[4] Karl Küpfmüller, Wolfgang Mathis, Albrecht Reibiger, Grundlagen der theoretischen Elektrotechnik, Springer-Verlag Berlin, Heidelberg, New York, 1978

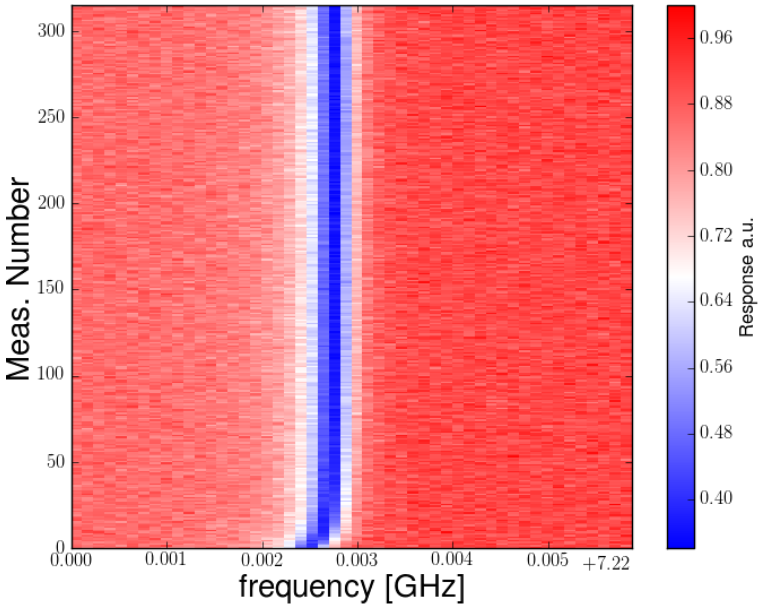

Figure 17: Change of the 7.22GHz transmission line during an LSM measurement

ETH

Eidgenössische Technische Hochschule Zürich
Swiss Federal Institute of Technology Zurich

Declaration of originality

The signed declaration of originality is a component of every semester paper, Bachelor's thesis, Master's thesis and any other degree paper undertaken during the course of studies, including the respective electronic versions.

Lecturers may also require a declaration of originality for other written papers compiled for their courses.

I hereby confirm that I am the sole author of the written work here enclosed and that I have compiled it in my own words. Parts excepted are corrections of form and content by the supervisor.

Title of work (in block letters):

Spatial Resolution of Current Distribution inside a Radio Frequency Resonator

Authored by (in block letters):
For papers written by groups the names of all authors are required.

Name(s):	**First name(s):**
Beckert	Adrian

With my signature I confirm that

- I have committed none of the forms of plagiarism described in the 'Citation etiquette' information sheet.
- I have documented all methods, data and processes truthfully.
- I have not manipulated any data.
- I have mentioned all persons who were significant facilitators of the work.

I am aware that the work may be screened electronically for plagiarism.

Place, date	**Signature(s)**
Zürich, 13.11.2014	

For papers written by groups the names of all authors are required. Their signatures collectively guarantee the entire content of the written paper.